The Thermal Decomposition of 1,2-Dioxetane Revisited

Sarah Wilsey,[§] Fernando Bernardi,[†] Massimo Olivucci,*[,†] Michael A. Robb,*[,§] Sean Murphy,[¶] and Waldemar Adam[¶]

Department of Chemistry, King's College London, Strand, London WC2R 2LS, U.K., Dipartimento di Chimica "G. Ciamician" dell'Universita di Bologna, Via Selmi 2, 40126 Bologna, Italy, and Institute für Organische Chemie, Universität Würzburg, Am Hubland, D-8700 Würzburg, FRG

Received: December 29, 1998

The ground state (S_0) and lowest energy triplet state (T_1) energy surfaces of the parent dioxetane have been extensively explored using various CASSCF active spaces with MP2 corrections in several basis sets. In particular, the singlet/triplet surface crossing regions have been examined and the spin−orbit coupling and energetics computed. The computed energy barrier for the ring-opening of dioxetane is 16 kcal mol^{-1}, which is lower than the experimentally observed threshold (22 kcal mol^{-1}) for unsubstituted dioxetane decomposition. However, the surface topology is in good agreement with the experimental observations. The barrier for O−O cleavage on the ground state surface is found to lie at nearly the same energy as the transition structure for C−C biradical cleavage on the triplet energy surface. More significantly, the computational results indicate that the singlet and triplet surfaces *do not cross* along the minimum energy path (MEP) between the ground state O−O cleavage transition state and the singlet biradical, as previously thought. Instead, the $S_0 \rightarrow {}^3(3\pi)$ surface crossing is prompted by a motion *orthogonal* to the reaction coordinate, which has components along both the OC−CO torsional and O−C−C asymmetric bending vibrational modes. In particular, we find evidence for a singlet/triplet crossing "line" that spans the ground state O−O cleavage valley and lies a few kcal mol^{-1} higher in energy. The computed spin−orbit coupling between the ground state and triplet $^3(3\pi)$ surfaces is large (ca. 60 cm^{-1}) throughout this crossing region. Therefore it is suggested that facile intersystem crossing (ISC) from the ground state to the triplet surface can occur anywhere along the MEP. ISC leads to production of a $^{\bullet}OCH_2-CH_2O^{\bullet}$ triplet biradical that can either fragment to form triplet products or undergo ISC back to the ground state surface. The existence of a triplet/singlet crossing region located very close to the computed triplet biradical, suggests that this species is metastable with a short (picosecond) lifetime.

Introduction

The thermal decomposition of 1,2-dioxetanes has received considerable attention in the past.[1,2] Most recently, accurate experimental investigations on simple methyl-substituted dioxetanes[3] have provided coherent information about the activation parameters and yields as a function of the degree and pattern of substitution. These data form an ideal basis for the formulation and testing of a detailed mechanism of chemienergization and luminescence. It is of particular interest that these compounds decompose on moderate heating (40−80 °C) to form a mixture of ground state, triplet, and a small amount of excited singlet carbonyl products. The large proportion (30−50%) of triplet product formed in symmetrically alkyl-substituted derivatives, such as tetramethyldioxetane[2] (TMD) and tetraethyldioxane[1] (TED), indicates that the thermally-induced singlet to triplet intersystem crossing (ISC) between the ground (S_0) and the first excited triplet state (T_1) must be extremely efficient. Fragmentation on the triplet energy surface then produces, in the case of the parent dioxetane, two molecules of formaldehyde, one in the ground state and one in the triplet ($n\pi^*$) state, as shown in Scheme 1. The excited state molecule can then decay radiatively with luminescence, although most of it decays nonradiatively.

Our initial theoretical study[4] of the mechanism for the decomposition of the parent dioxetane molecule predicted the energy diagram shown in Figure 1a. According to this diagram, the rate-determining step on the ground state surface corresponds to oxygen−oxygen (O−O) cleavage into a $^{\bullet}OCH_2-CH_2O^{\bullet}$ biradical, analogous to the accepted "textbook" mechanism (Figure 1b).[5,6] However, Figure 1a suggests that the activation energy for O−O cleavage on the ground state surface is very small (ca. 3 kcal mol^{-1}). Further, while the ground state product formation is controlled by this small barrier, the activation energy for $^{\bullet}OCH_2-CH_2O^{\bullet}$ biradical fragmentation on the T_1 energy surface is found to be 20 kcal mol^{-1} higher. This predicts that the ground and excited state pathways must have very different activation energies. On reviewing the experimental data on dioxetanes, the computed energy diagram appears to be inconsistent with the following independent observations: (a) the barrier for the rate-determining step in the unsubstituted

SCHEME 1

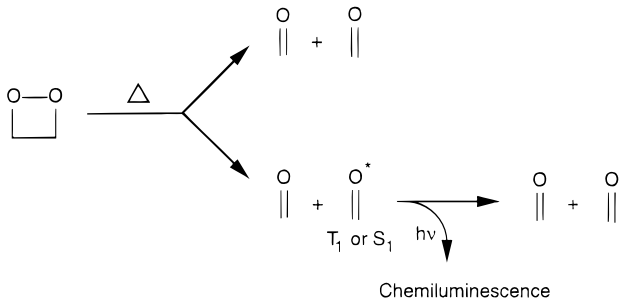

[§] King's College London.
[†] Universita di Bologna.
[¶] Universität Würzburg.

10.1021/jp9848086 CCC: $18.00
Published on Web 02/25/1999

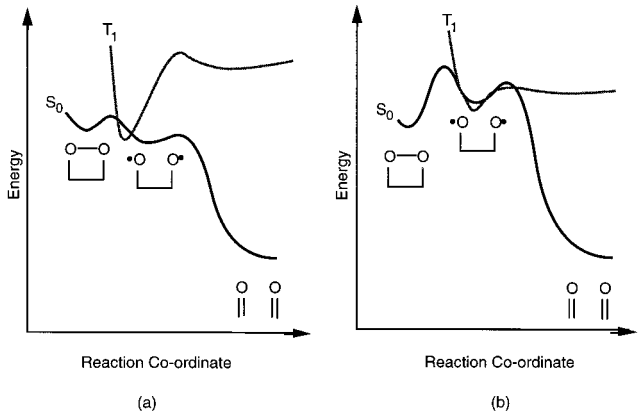

Figure 1. Energy diagrams for dioxetane decomposition on the singlet (S_0) and triplet (T_1) state surfaces: (a) energy diagram computed in ref 4; (b) "textbook" energy diagram, refs 5 and 6.

dioxetane[3] is 22 kcal mol^{-1}; (b) measurements on TMD[1,7] and *cis*-diethoxy-1,2-dioxetane[8] (DED) indicate that the activation energy for the ground state (singlet) and excited state (triplet) decomposition reactions are the same; (c) for 3,3-dimethyl-1,2-dioxetane[9] the lack of trapping establishes that the lifetime of the triplet biradical intermediate must be very short (<10 ps).

In order to eliminate the discrepancy between the computed[10] and experimentally derived mechanistic pictures, we have reinvestigated both the singlet and triplet dioxetane decomposition pathways using several different high level computational methods. We have mapped out the different singlet and triplet potential energy surfaces and studied possible singlet/triplet crossing regions, using spin−orbit coupling (SOC) computations to predict the efficiency of ISC.

The new results are summarized in Figure 2a. Clearly, in spite of the much improved agreement with experiment for the energetics, the computed singlet O−O cleavage barrier (about 17.6 kcal/mol uncorrected, 16.3 kcal mol^{-1} when thermally corrected) is still underestimated with respect to the experimentally observed barrier of 22 kcal mol^{-1}. Further, while the computed singlet O−O cleavage and triplet C−C fragmentation barriers (corresponding to **TS$_1$** and **TS$_2$** in Figure 2a) are of the same magnitude, we find that the ground state and $^3(3\pi)$ state energy surfaces are separated by a gap of a few kcal mol^{-1}, which persists along the path to the singlet biradical (**BIR^S**). It is therefore unclear how the $^3(^3\pi)$ state is efficiently populated via O−O cleavage.

In the following sections we describe how the discrepancy between computational and experimental results can be substantially reduced by moving from a one-dimensional to a two-dimensional view of the reaction coordinate. In particular, we show that some 6 kcal mol^{-1} above the O−O cleavage transition structure there is a T_1/S_0 energy surface crossing that extends along the path to the biradical region. This $n-1$-dimensional crossing surface (where n is the number of degrees of freedom in the molecule) provides an efficient ISC channel to the $^3(3\pi)$ surface, such that O−O cleavage becomes the rate-determining step for production of both singlet and triplet products. This is consistent with observation (b). We explain the origin of observation (c) on the basis of the computed energy surfaces in the biradical region (see Figure 2c), where we have identified a crossing region in the vicinity of the triplet $^3(3\pi)$ biradical, **BIR^T**, where ISC back to the ground state surface can occur. The large computed spin−orbit coupling (SOC) of ca. 60 cm^{-1} in this crossing region suggests that this ISC will be exceedingly

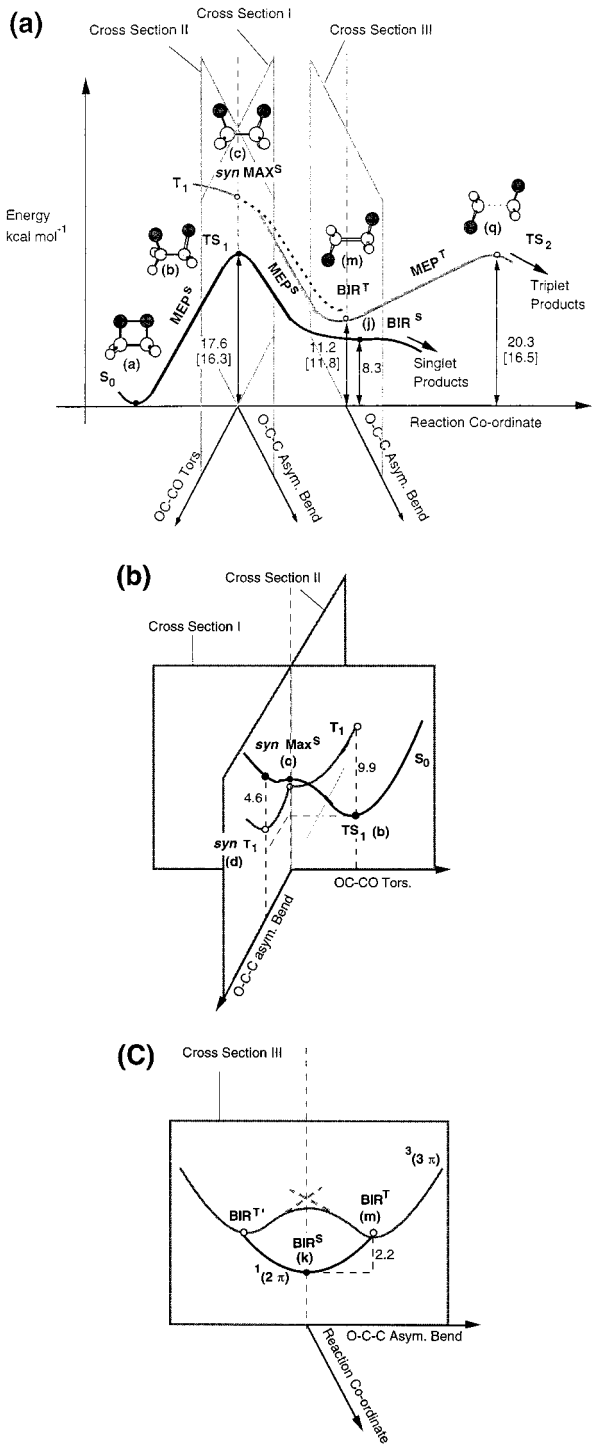

Figure 2. Recomputed energy diagram for dioxetane decomposition on the ground state and triplet $^3(3\pi)$ surfaces using state-of-the-art *ab initio* computations. All energy values are given in kcal mol^{-1}. The labels refer to the structures shown in Figure 3. The energies are from Table 2. (a) One-dimensional energy diagram of the ground state and triplet $^3(3\pi)$ potential energy surfaces along the dioxetane decomposition reaction coordinate computed using CAS(12,10)/6-31+G*+MP2 with thermally corrected values in square brackets. (b) Potential energy diagram of the singlet $^1(4\pi)$ and triplet $^3(3\pi)$ potential energy surfaces along the **TS$_1$**-*syn* **MAX^S** OC−CO twisting coordinate and along the *syn* **MAX^S**-*syn* **T$_1$** O−C−C asymmetric bending coordinate, orthogonal to the reaction coordinate in the O−O cleavage region. Energies computed at the CAS(8,6)/6-31G*+MP2 level. (c) One-dimensional energy diagram of the ground state $^1(2\pi)$ and triplet $^3(3\pi)$ potential energy surfaces along the **BIR$^{T'}$**-**BIR^S**-**BIR^T** O−C−C asymmetric bending coordinate, orthogonal to the reaction coordinate in the biradical region. Energies are computed at the CAS(8,6)/6-31G*+MP2 level.

CHART 1

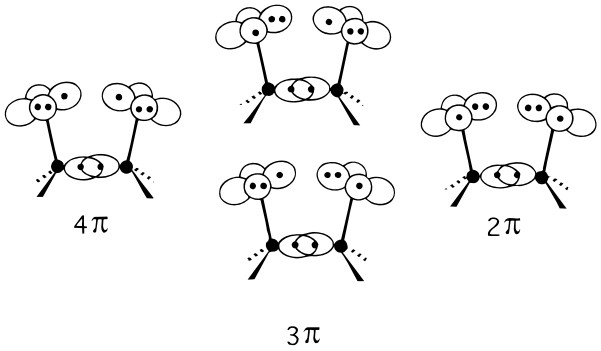

fast, such that **BIR^T** can be regarded as a metastable species with a picosecond lifetime, too short-lived for chemical trapping.

Theoretical Background and Computational Details

It is usually assumed[9,11] that dioxetane decomposition takes place via biradical intermediates $^{\bullet}OCH_2-CH_2O^{\bullet}$ formed after initial cleavage of the O−O bond. Due to the weak interaction between the two radical centers, especially in the *anti* conformation, such a biradical is electronically rather complex since there is a possible 8-fold (4-fold triplet and 4-fold singlet) state quasi-degeneracy. The quasi-degeneracy arises from the different possible occupations of the orbitals on the oxygen atoms (Chart 1).

The two states of most interest are the singlet 4π electron state ($^1(4\pi)$), which describes the reactant and ground state products, and the triplet 3π electron state ($^3(3\pi)$), which describes the triplet excited state products (i.e., a mixture of triplet and ground state formaldehyde). The small quantity of excited state singlet formaldehyde that has also been observed[1−3] would result from dissociation from the singlet 3π electron state ($^1(3\pi)$). The third possible orbital configuration corresponds to the singlet and triplet 2π electron states; dissociation from these surfaces would lead to two excited state formaldehyde molecules, which would occur at much higher energies.

The exploratory computations of Reguero *et al.*[4] on the singlet and triplet potential surfaces of dioxetane were performed using complete active space (CAS)-SCF with a limited active space and a 4-31G basis set. Our primary objectives in this work are to investigate the potential energy surface for the decomposition of dioxetane in more detail using higher levels of theory and to document the regions of the reaction coordinate (for both the O−O cleavage and fragmentation steps) where the $^3(3\pi)$ triplet surface crosses with the ground state surface. The relative energies of the minima and transition states on the ground state and $^3(3\pi)$ surfaces of dioxetane are the central question. Therefore, we have computed these quantities using a hierarchy of methods (CASSCF, GVBCAS, and multireference MP2) with various basis sets, in order to demonstrate some convergence in the computational results.

An active space of eight electrons in six orbitals (Chart 1) is the minimum needed to describe the topology of the potential surfaces involved. These energetics can be corrected by performing multireference MP2 (CASMP2) computations using this CASSCF reference space. However, it is not possible to perform geometry optimizations using CASMP2. Therefore, an improved level of theory requires increasing the active space by adding additional orbitals so that some of the dynamic correlation effects can be included in the CASSCF geometry optimization. The obvious extension of the active space involves the inclusion of the C−O σ/σ^* orbitals to give a CAS(12,10)

CHART 2

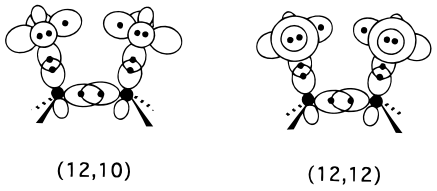

space (see Chart 2). The addition of a pair of "virtual" n* orbitals yields a (12,12) space, although this active space is too large for CASSCF geometry optimizations. In such cases, the structures were optimized using GVBCAS calculations, in which the four C−O σ orbitals were kept in the GVB space. CAS-(8,8)/MP2 energies (without the σ,σ^* orbitals) were then computed at these structures.

The standard GAUSSIAN[12] 6-31G* basis set was used for the routine CAS(8,6) and GVBCAS(12,12) computations, while the CAS(12,10) computations were run with the 6-31+G* basis. The barrier heights for the ground state O−O cleavage transition state and the triplet dissociation transition state were also recomputed in the CAS(8,6) active space using the correlation consistent cc-pVDZ basis set of Dunning. These calculations were expected to give more reliable energetics, since the s and p orbitals are contracted separately, and the basis sets have been optimized using a correlated wavefunction. In each case the results were corrected with single point multireference MP2 computations, using the method of Peasley *et al.*[13] (CASMP2) for the (8,6) and (8,8) active spaces, and the method of Roos[14] (CASPT2) for the (12,10) active space. These MP2 methods differ mainly in the choice of zeroth-order Hamiltonian.

Frequency calculations were carried out at each of the critical points located at the CASSCF/6-31G* level, using a (4,4) active space without the doubly occupied oxygen orbitals. These were used both to verify the nature of the point found and to provide zero-point energy (ZPE) corrections. At a few selected points (**a**, **b**, **m**, and **q**), frequencies were computed using an (8,6) active space for extra accuracy, and these were used for evaluating thermal corrections (including ZPE) to the energies at these points (see Table 1). In some regions of the potential energy surface, near-degeneracies between surfaces led to unreliable frequency computations, and these are indicated in the table.

Crossing points were located using the conical intersection algorithm in GAUSSIAN94.[12] This method optimizes the lowest energy point on an $n-2$-dimensional intersection hyperline between two surfaces of the same symmetry and multiplicity. The remaining two dimensions describe a plane spanned by the derivative coupling and gradient difference vectors. Such a method has been the focus of several papers[15] recently, and therefore is not described in detail here. Spin−orbit coupling calculations were performed using the code implemented in GAUSSIAN94. This code uses a one-electron approximation for the spin−orbit coupling operator, with the effective nuclear charges of Koseki *et al.*[16] (C, 3.6; O, 5.6). For both the conical intersection optimizations and the spin−orbit coupling computations, state-averaged orbitals were used.

Results and Discussion

The relevant energetics for the minima and transition states on the triplet and singlet potential energy surfaces along the dioxetane decomposition reaction coordinate are collected in Tables 1 and 2, and the corresponding molecular structures are shown in Figure 3. Several conical intersection structures were

TABLE 1: CAS-SCF and Multireference MP2 Energies for Dioxetane Decomposition Potential Energy Surfaces

structure (see Figure 3)	state (see Chart 1)	CAS (8,6)/ 6-31G* [a]	CAS (8,6)/ 6-31G*+MP2[a]	relative ZPE correction[b]	relative thermal correction[b]
dioxetane					
(a)	$S_0\ ^1(4\pi)$	−227.6988	−228.2221 **(0.0)**	**(0.0)**	**(0.0)**
TS_1					
(b)	$S_0\ ^1(4\pi)$	−227.6863	−228.1950 **(17.0)**	**(−1.1)**	**(−1.3)**
	$T_1\ ^3(3\pi)$	−227.6703	−228.1792 **(26.9)**		
syn **MAX^S**					
(c)	$S_0\ ^1(4\pi)$	−227.6819	−228.1853 **(23.1)**	**(+1.9)**	
	$T_1\ ^3(3\pi)$	−227.6824	−228.1882 **(21.3)**		
syn **T_1**					
(d)	$T_1\ ^3(3\pi)$	−227.6869[c]	−228.1912 **(19.4)**	*e*	
	$S_1\ ^1(4\pi)$	−227.6802	−228.1839 **(24.0)**		
gauche **BIR**					
(e)	$S_0\ ^1(4\pi)$	−227.6952	−228.2007 **(13.4)**	**(−1.6)**	
	$S_2\ ^1(2\pi)$	−227.6933	−228.1995 **(14.2)**		
	$T_1\ ^3(3\pi)$	−227.6931	−228.2000 **(13.9)**		
(f)	$S_0\ ^1(2\pi)$	−227.6980	−228.2052 **(10.6)**	**(−2.3)**	
	$S_1\ ^1(4\pi)$	−227.6912	−228.1965 **(16.1)**		
	$T_2\ ^3(3\pi)$	−227.6935	−228.1994 **(14.2)**		
(g)	$T_1\ ^3(2\pi)$	−227.6978	−228.2052 **(10.6)**	**(−2.4)**	
(h)	$T_2\ ^3(3\pi)$	−227.6954[c]	−228.2039[d] **(11.4)**	*e*	
	$S_0\ ^1(2\pi)$	−227.6959	−228.2041 **(11.3)**		
	$S_2\ ^1(4\pi)$	−227.6931	−228.1986 **(14.7)**		
(i)	$S_1\ ^1(3\pi)$	−227.6951[c]	−228.2033[d] **(11.8)**	*e*	
anti **BIR**					
(j)	$S_0\ ^1(4\pi)$	−227.6964	−228.2021 **(12.6)**	**(−1.8)**	
	$S_2\ ^1(2\pi)$	−227.6919	−228.1986 **(14.7)**		
	$T_1\ ^3(3\pi)$	−227.6930	−228.1986 **(14.7)**		
(k)	$S_0\ ^1(2\pi)$	−227.6990	−228.2074 **(9.2)**	**(−2.0)**	
	$S_2\ ^1(4\pi)$	−227.6913	−228.1965 **(16.1)**		
(l)	$T_1\ ^3(2\pi)$	−227.6990	−228.2073 **(9.3)**	**(−2.5)**	
(m)	$T_2\ ^3(3\pi)$	−227.6960[c]	−228.2039[d] **(11.4)**	**(+0.4)**	**(+0.6)**
	$S_0\ ^1(2\pi)$	−227.6972	−228.2045 **(11.1)**		
	$S_2\ ^1(4\pi)$	−227.6939	−228.1995 **(14.2)**		
(n)	$S_1\ ^1(3\pi)$	−227.6956[c]	−228.2032[d] **(11.9)**	*e*	
gauche **TS_2**					
(o)	$S_0\ ^1(4\pi)$	−227.6960[c]	−228.2007 **(13.4)**	**(−2.7)**	
(p)	$T_1\ ^3(3\pi)$	−227.6644	−228.1782 **(27.5)**	**(−4.5)**	
anti **TS_2**					
(q)	$T_1\ ^3(3\pi)$	−227.6666	−228.1813 **(25.6)**	**(−4.4)**	**(−3.8)**

[a] Absolute energies in Hartrees with energies in kcal mol^{-1} relative to those of the S_0 reactant in parentheses. [b] Energies in kcal mol^{-1} relative to the S_0 reactant. [c] Structure not completely optimized in full active space. [d] MP2 calculation in (4,4) active space. [e] Frequency calculation unreliable due to near degeneracies of other states.

TABLE 2: Energies Computed at GVB-CAS(12,12)/6-31G*, CAS(8,8)/6-31G* + MP2, CAS(8,6)/cc-pVDZ + MP2, and CAS (12,10)/6-31+G* + MP2 Levels of Theories for a Series of Relevant Structures[a]

structure (see Figure 3)	state (see Chart 1)	GVB-CAS (12,12)/6-31G*	CAS (8,8)/ 6-31G* + MP2[b]	CAS (8,6)/ cc-pVDZ	CAS (8,6)/ cc-pVDZ+MP2	CAS (12,10)/ 6-31+G*	CAS (12,10)/ 6-31+G* + MP2	CAS (12,10)/ 6-31+G* + MP2 + thermal
dioxetane								
(a)	$S_0\ ^1(4\pi)$	−227.7828	−228.2349 **(0.0)**	−227.7145	−228.2597 **(0.0)**	−227.7807	−228.2975 **(0.0)**	**(0.0)**
TS_1								
(b)	$S_0\ ^1(4\pi)$	−227.7557	−228.2064 **(17.9)**	−227.7029	−228.2331 **(16.7)**	−227.7526	−228.2514 **(17.6)**	**(16.3)**
anti **BIR**								
(j)	$S_0\ ^1(4\pi)$					−227.7607	−228.2662 **(8.3)**	
(m)	$T_2\ ^3(3\pi)$					−227.7605	−228.2617 **(11.2)**	**(11.8)**
	$S_2\ ^1(4\pi)$					−227.7577	228.2601 **(12.2)**	
anti **TS_2**								
(q)	$T_1\ ^3(3\pi)$	−227.7355	−228.1931 **(25.6)**	−227.6850	−228.2241 **(22.4)**	−227.7422	−228.2472 **(20.3)**	**(16.5)**

[a] Absolute energies in Hartrees with energies in kcal mol^{-1} relative to those of the S_0 reactant in parentheses. [b] Computed at the GVB-CAS(12,12)/6-31G* geometries.

also optimized; these are illustrated in Figure 4 with the corresponding energies in Table 3. As mentioned in the previous section, the two potential energy surfaces of most interest for the reaction mechanism are those of the $^1(4\pi)$ and $^3(3\pi)$ states. Accordingly, a schematic energy diagram of the reaction pathways on these energy surfaces is shown in Figure 2a (the energetics in this figure have been calibrated for a set of selected structures (**a**, **b**, **j**, **m**, and **q**) computed at the CAS(12,10)/6-31+G*+MP2 levels of theory). However, as we shall discuss in detail below, other electronic states become involved in the region of the singlet and triplet $^{\bullet}OCH_2-CH_2O^{\bullet}$ biradicals (here generically indicated by **BIR^S** and **BIR^T**).

The ground state ($^1(4\pi)$) O−O cleavage transition state **TS_1** (structure **b**) corresponds to a *gauche* structure with an activation energy of ca. 17.6 kcal mol^{-1} (16.3 kcal mol^{-1} with thermal correction). Structure **c** corresponds to a $^1(4\pi)$ second-order saddle point (*syn* **MAX^S**) located some 6 kcal mol^{-1} above **TS_1**. At this point the triplet $^3(3\pi)$ energy surface was found to lie

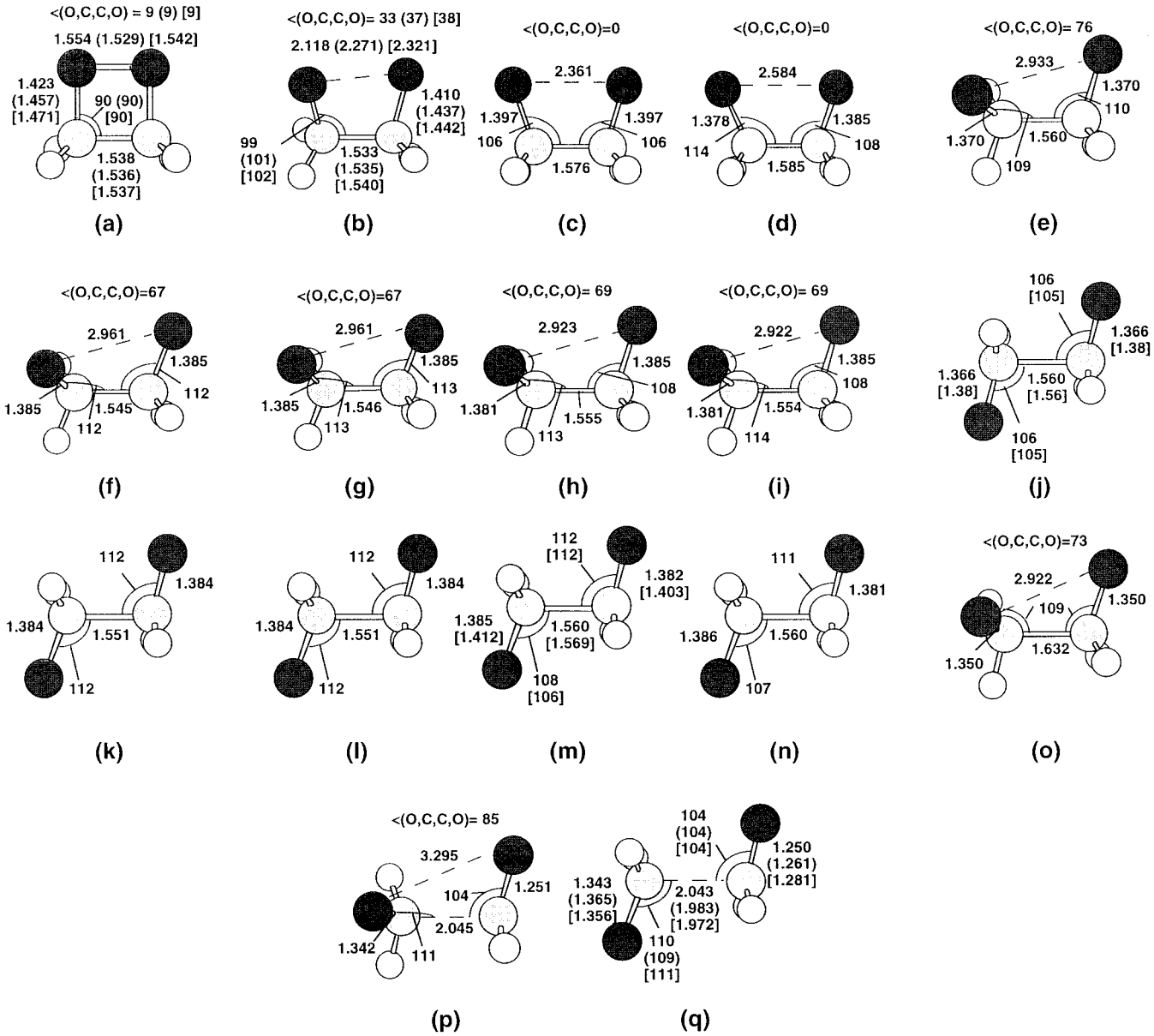

Figure 3. Optimized molecular structures for (a) dioxetane, (b) S_0 $^1(4\pi)$ O−O cleavage transition state (**TS$_1$**), (c) S_0 $^1(4\pi)$ *syn* second-order saddle point (*syn* **MAX^S**), (d) T_1 $^3(3\pi)$ *syn* maximum (*syn* **T$_1$**), (e) S_0 $^1(4\pi)$ *gauche* biradical (**BIR^S**) (C−C bond length constrained), (f) S_0 $^1(2\pi)$ *gauche* biradical, (g) T_1 $^3(2\pi)$ *gauche* biradical, (h) T_2 $^3(3\pi)$ *gauche* biradical (**BIR^T**), (i) S_1 $^1(3\pi)$ *gauche* biradical, (j) S_0 $^1(4\pi)$ *anti* biradical (**BIR^S**) (C−C bond length constrained), (k) S_0 $^1(2\pi)$ *anti* biradical (**BIR^S**), (l) T_1 $^3(2\pi)$ *anti* biradical, (m) T_2 $^3(3\pi)$ *anti* biradical (**BIR^T**), (n) S_1 $^1(3\pi)$ singlet *anti* biradical (o) S_0 $^1(4\pi)$ *gauche* fragmentation transition state, (p) T_1 $^3(3\pi)$ *gauche* fragmentation transition state (**TS$_2$**), and (q) T_1 $^3(3\pi)$ *anti* fragmentation transition state (**TS$_2$**). Bond lengths are given in angstroms, and angles in degrees.

ca. 2 kcal mol^{-1} *lower* in energy than the $^1(4\pi)$ surface (to be discussed in detail subsequently). The lowest (4π) biradical (**BIR^S** in Figure 2a) has an *anti* conformation (structure **j**) and is located 9 kcal mol^{-1} below **TS$_1$**. This biradical is unstable with respect to C−C cleavage such that a fragmentation barrier could not be fully optimized. The *anti* minimum (structure **m**) on the $^3(3\pi)$ energy surface (**BIR^T** in Figure 2a) is located 5−6 kcal mol^{-1} below **TS$_1$**. At the best level of theory used (CAS-(12,10)/6-31+G* + MP2 + thermal correction), the T_1 $^3(3\pi)$ *anti* biradical fragmentation transition state **TS$_2$** (structure **q**) lies 20.3 kcal mol^{-1} above the reactant molecule (16.5 kcal mol^{-1} when thermally corrected). The thermal correction is larger in **TS$_2$** than **TS$_1$**, as expected, as **TS$_2$** is a much looser transition state (see Tables 1 and 2), such that both **TS$_1$** and **TS$_2$** correspond to barriers of around 16.5 kcal mol^{-1}.

The one-dimensional diagram of Figure 2a supports a mechanism for dioxetane decomposition where there is (i) an activation energy of around 16.5 kcal mol^{-1}, (ii) a very unstable $^1(4\pi)$ biradical intermediate **BIR^S** that can fragment immediately, (iii) a triplet $^3(3\pi)$ biradical intermediate **BIR^T**, and (iv) a triplet fragmentation barrier **TS$_2$** that is of the same magnitude as the S_0 O−O cleavage barrier, **TS$_1$**. These data provide a much better agreement with experiment as compared to the previous computational work.[4] However, the computed barrier for the rate-determining step still remains some 6 kcal mol^{-1} less than the experimental activation energy.[3] Furthermore, no clear-cut mechanism for the production of the triplet intermediate **BIR^T** emerges from the one dimensional diagram of Figure 2a. In particular, no $S_0 \rightarrow {}^3(3\pi)$ crossing occurs along the ground state O−O cleavage reaction path.

In the following section we show that, while the computed barrier height remains in disagreement with experiment (i.e., CASMP2 appears to underestimate the stability of the closed four-membered ring), the formulation of a consistent mechanism

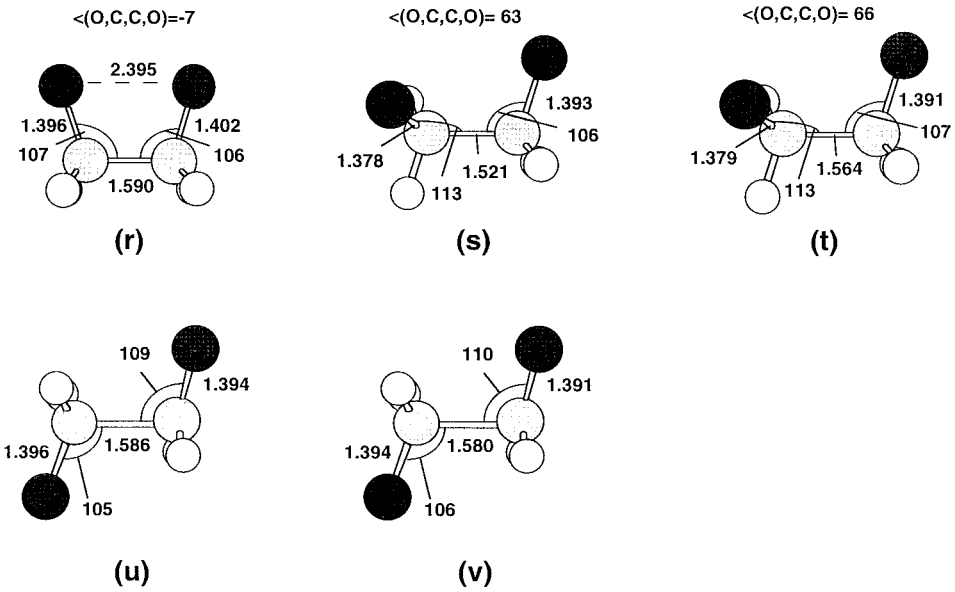

Figure 4. Optimized crossing points: (r) $^1(4\pi)/^1(3\pi)$ conical intersection near *syn* **MAX^S**; (s) $^1(2\pi)/^1(3\pi)$ crossing point in the region of the (3π) *gauche* biradical minima; (t) $^3(2\pi)/^3(3\pi)$ crossing point in the region of (3π) *gauche* biradical minima; (u) $^1(2\pi)/^1(3\pi)$ crossing point in the region of the (3π) *anti* biradical minima; (v) $^3(2\pi)/^3(3\pi)$ crossing point in the region of the (3π) *anti* biradical minima.

TABLE 3: CAS-SCF Energies for Crossing Points on the Dioxetane Decomposition Potential Energy Surfaces[a]

structures (see Figure 4)	state (see Chart 1)	CAS (8,6)/ 6-31G* (Hartrees)	relative energy (kcal/mol)
dioxetane **(a)**	S_0 $^1(4\pi)$	−227.6988	**0.0**
TS_1 (b)	S_0 $^1(4\pi)$	−226.6963	**+7.8**
S_0/S_1 crossing near *syn* **MAX^S (r)**	S_0 $^1(4\pi)$	−227.6811	**+11.1**
	S_1 $^1(3\pi)$	−227.6810	**+11.2**
	T_1 $^3(3\pi)$	−227.6818‡	**+10.7**
	T_1 $^3(3\pi)$	−227.6829§	**+10.0**
S_0/S_1 crossing near *gauche* **BIR (s)**	S_0 $^1(2\pi)$	−227.6937	**+3.2**
	S_1 $^1(3\pi)$	−227.6934	**+3.4**
	T_1 $^3(2\pi)$	−227.6939	**+3.1**
	T_2 $^3(3\pi)$	−227.6934	**+3.4**
T_1/T_2 crossing near *gauche* **BIR (t)**	T_1 $^3(2\pi)$	−227.6948	**+2.5**
	T_2 $^3(3\pi)$	−227.6943	**+2.8**
	S_0 $^3(2\pi)$	−227.6950	**+2.4**
	S_1 $^3(3\pi)$	−227.6938	**+3.1**
S_0/S_1 crossing near *anti* **BIR (u)**	S_0 $^1(2\pi)$	−227.6936	**+3.3**
	S_1 $^1(3\pi)$	−227.6935	**+3.3**
	T_1 $^3(2\pi)$	−227.6941	**+2.9**
	T_2 $^3(3\pi)$	−227.6933	**+3.5**
T_1/T_2 crossing near *anti* **BIR (v)**	T_1 $^3(2\pi)$	−227.6946	**+2.6**
	T_2 $^3(3\pi)$	−227.6946	**+2.6**
	S_0 $^3(2\pi)$	−227.6949	**+2.4**
	S_1 $^3(3\pi)$	−227.6940	**+3.0**

[a] Energies obtained using state-averaged orbitals over two states, with weights 0.5:0.5, except for T_1 at point **r**, which was computed both by state-averaging over three states with weights 0.33:0.33:0.34 (marked ‡) and without state-averaging (marked §).

for dioxetane decomposition and chemienergization can be derived by moving from a one-dimensional to a two-dimensional view of the reaction coordinate. In particular, we show that efficient production of the $^3(3\pi)$ intermediates can be explained by motion through a vast $S_0/^3(3\pi)$ crossing region that spans the O−O cleavage valley connecting **TS_1** and **BIR^S**. This crossing region cannot be detected simply by following the O−O cleavage minimum energy path, since it is located a few kcal mol^{-1} higher in energy, and can only be intercepted by a motion *orthogonal* to the reaction coordinate.

Structure of the O−O Cleavage Transition State Region. Our purpose in this subsection is to demonstrate that many energetically accessible $^1(4\pi)/^3(3\pi)$ crossings, induced by O−C−C asymmetric bending and OC−CO torsional deformations, are located near the O−O cleavage transition state region. Figure 2b shows cross-sections in the region of **TS_1** along these O−C−C asymmetric bending and OC−CO torsional deformations. Motion along the OC−CO torsional coordinate from **TS_1** leads to a symmetric second-order saddle point, *syn* **MAX^S** (structure **c**), where the $^3(3\pi)$ state lies below the $^1(4\pi)$ state. Motion along an in-plane asymmetric bending from *syn* **MAX^S** leads to *syn* **T_1** (structure **d**) where the $^3(3\pi)$ state lies even further below the singlet surface in energy. We now discuss this crossing region in more detail.

The ground state O−O cleavage transition state **TS_1** (structure **b**) has a 33° twisted structure, and there is an equivalent (i.e., mirror-image) transition state **TS_1'** with a −33° twist. These two transition states are connected via the OC−CO twisting coordinate that is *orthogonal* to the O−O cleavage reaction coordinate (see Figure 2a,b). The computed $^1(4\pi)$ energy profile the OC−CO twisting coordinate corresponds to a double well, where **TS_1** and **TS_1'** form the two *gauche* "minima" of the double well, with a planar, symmetric structure, *syn* **MAX^S** (structure **c**), located at the double well maximum. This stationary point (a local energy maximum with two imaginary frequencies: 1117i cm^{-1} corresponding to O−O stretching and 192i cm^{-1} corresponding to OC−CO torsion) was fully optimized and lies 6.1 kcal mol^{-1} above the energy of the two transition states (see Table 1). At **TS_1** and **TS_1'** the triplet $^3(3\pi)$ surface lies 9.9 kcal mol^{-1} *above* the energy of the singlet $^1(4\pi)$ surface (see Figure 6 in the Supporting Information for details). However, at the local maximum, *syn* **MAX^S**, the triplet $^3(3\pi)$ surface lies 1.8 kcal mol^{-1} *below* the $^1(4\pi)$ surface (see Table 1). Thus, the $^3(3\pi)$ and $^1(4\pi)$ potential energy surfaces cross in the O−O cleavage region between **TS_1** and *syn* **MAX^S**. Since the computed SOC at the crossing points is very large in this region (ca. 60 cm^{-1}), there is an efficient ISC channel from the $^1(4\pi)$ surface to the $^3(3\pi)$ surface. Attempts to optimize the lowest energy $^1(4\pi)/^3(3\pi)$ crossing point were thwarted by the presence of the $^1(3\pi)$ surface, which lies very close in energy to the $^3(3\pi)$ surface. However, a $^1(4\pi)/^3(3\pi)$ conical intersection (structure **r** in Figure 4) was located only 3.3 kcal mol^{-1} above

TS_1. At this point the triplet $^3(3\pi)$ surface lies only 1 kcal mol^{-1} below the $^1(4\pi)$ surface, suggesting the $^3(3\pi)/^1(4\pi)$ crossing is close.

A planar stationary point *syn* $\mathbf{T_1}$ (structure **d**) of biradical nature was also located on the $^3(3\pi)$ surface close to *syn* $\mathbf{MAX^S}$, but at an asymmetric geometry. This structure was optimized as a transition state corresponding to OC−CO torsion. The frequency calculation indicated two imaginary frequencies but is unreliable due to the near degeneracy of the other triplet 3π state. This structure lies only 2.4 kcal mol^{-1} above $\mathbf{TS_1}$. At this structure the $^3(3\pi)$ surface lies 4.6 kcal mol^{-1} below the $^1(4\pi)$ surface in energy.

Thus, Figure 2b shows that while an out-of-plane deformation of the highly symmetric *syn* $\mathbf{MAX^S}$ structure (i.e., a deformation toward $\mathbf{TS_1}$) leads to stabilization of the $^1(4\pi)$ state with respect to the $^3(3\pi)$ state, an in-plane asymmetric bending motion from the *syn* $\mathbf{MAX^S}$ structure (i.e., a deformation toward *syn* $\mathbf{T_1}$) greatly stabilizes the $^3(3\pi)$ state. Therefore, the O−O cleavage transition state region must be spanned by many energetically accessible $^1(4\pi)/^3(3\pi)$ crossings, induced by O−C−C asymmetric bending and OC−CO torsional deformations.

The Biradical Region. The S_0 to T_1 and T_1 to S_0 Channels. In Figure 2a we show that a ground state minimum energy path ($\mathbf{MEP^S}$) connects the O−O cleavage transition state $\mathbf{TS_1}$ (structure **b**) to the $^1(4\pi)$ *anti* biradical minimum $\mathbf{BIR^S}$. While this is qualitatively correct, the computed $\mathbf{MEP^S}$ has a considerably more complex structure. In fact, the $\mathbf{MEP^S}$ coordinate starting at $\mathbf{TS_1}$ terminates in the vicinity of a stable *gauche* biradical minimum on the singlet $^1(2\pi)$ potential energy surface (structure **f**), as the $^1(4\pi)$ and $^1(2\pi)$ surfaces cross along the $\mathbf{MEP^S}$ coordinate. This coordinate retains C_2 symmetry and corresponds mainly to an increase in the OC−CO torsional angle from 33° to 67°. Further motion along this torsional coordinate into the region of the *anti* conformers leads to the lowest energy singlet biradical, which is again a $^1(2\pi)$ structure (structure **k**), stable to C−C cleavage. However, a C−C stretching motion from either *gauche* or *anti* $^1(2\pi)$ biradicals (i.e., a fragmentation motion) leads to the $^1(4\pi)$ gauche $\mathbf{BIR^S}$ (structure **e**) and $^1(4\pi)$ *anti* $\mathbf{BIR^S}$ (structure **j**) respectively. These had to be optimized with constrained C−C distances (1.56 Å), as they are unstable to C−C fission. This is consistent with the fact that the $^1(4\pi)$ state is the only one that correlates with two molecules of ground state formaldehyde.

The $^3(3\pi)$ biradicals, $\mathbf{BIR^T}$, were located at both *gauche* (structure **h**) and *anti* (structure **m**) geometries. These structures could only be optimized in a (4,4) active space, as the $^3(2\pi)$ surface is virtually degenerate at these points. While the *gauche* structure was optimized as a minimum, the frequency calculation showed one imaginary frequency but is unreliable due to the near degeneracy of the $^3(2\pi)$ surface. The *anti* structure had no imaginary frequencies. Notice that *syn* $\mathbf{T_1}$ (structure **d**) corresponds to a conformational transition state between the two *gauche* $^3(3\pi)$ biradicals.

The main structural differences between the $^1(4\pi)$ $\mathbf{BIR^S}$ and the $^3(3\pi)$ $\mathbf{BIR^T}$ biradicals can be seen by comparing the different *gauche* (**e** and **h**) and *anti* (**j** and **m**) structures. The triplet biradicals have only one tight O−C−C bending angle and slightly longer C−O bonds. In fact, lower symmetry is a general feature of the molecular geometries on the $^3(3\pi)$ energy surface (see for instance structures **d**, **h**, **m**, **p**, and **q**). Therefore, along the symmetric $\mathbf{MEP^S}$, the 3π geometries are unstable and the 2π and 4π geometries are stable. On the other hand, at asymmetric geometries the 3π geometries are stable, while the 2π and 4π geometries are unstable. This leads to the type of surface topology depicted in cross-sections II and III shown in Figure 2b,c, respectively.

In the regions around the triplet $^3(3\pi)$ biradicals $\mathbf{BIR^T}$, the ground state surface is the $^1(2\pi)$ surface and the lowest energy triplet surface is the $^3(2\pi)$ surface, although all four surfaces are virtually degenerate in the region of the $^3(3\pi)$ minima. The structure of the $^3(3\pi)$ and $S_0{}^1(2\pi)$ potential energy surfaces along the coordinate connecting $\mathbf{BIR^T}$ (and the mirror image biradical $\mathbf{BIR^{T'}}$) to the *anti* $^1(2\pi)$ minimum is illustrated in Figure 2c. The deformation between the two biradical minima is an O−C−C asymmetric bending motion, orthogonal to the reaction coordinate (see cross-section III in Figure 2a,c), analogous to the motion connecting *syn* $\mathbf{MAX^S}$ and *syn* $\mathbf{T_1}$ (Figure 2b). Although a $^3(3\pi)/^1(2\pi)$ crossing could not be optimized, both $^1(3\pi)/^1(2\pi)$ (structures **s** and **u**) and $^3(3\pi)/^3(2\pi)$ (structures **t** and **v**) crossing points were located at asymmetric geometries close to the *gauche* and *anti* $^3(3\pi)$ minima. The spin−orbit coupling computed between 3π and 2π surfaces with different spin was found to be large (69−70 cm^{-1}). The ground state $^1(2\pi)$ surface is lower in energy than the $^3(3\pi)$ surface; therefore facile ISC can occur from $\mathbf{BIR^T}$ back to the ground state surface such that the triplet biradical intermediate is expected to have a very short lifetime.

In previous theoretical work, Harding and Goddard[17] reported a 3.1 kcal mol^{-1} dispersion for the eight low-lying states in the biradical region. Our results are consistent with this result as we have located stable *gauche* and *anti* minima on the $^1(2\pi)$ surface (structures **f** and **k**) coincident with minima on the $^3(2\pi)$ surface (structures **g** and **l**), all with C_2 symmetry; and *gauche* and *anti* minima on the $^3(3\pi)$ surface (structures **h** and **m**) coincident with minima on the $^1(3\pi)$ surface (structures **i** and **n**) at *asymmetric* geometries. Both unstable *gauche* (structure **e**) and *anti* (structure **j**) minima were located on the $^1(4\pi)$ surface, although these had to be optimized with constrained C−C distances as the surface is very flat with respect to C−C fission.

Therefore, a vast biradical multistate degeneracy extends along the S_0 valley between $\mathbf{TS_1}$ and $\mathbf{BIR^S}$. The $^1(4\pi)$ and $^1(2\pi)$ surfaces cross along $\mathbf{MEP^S}$, and then recross as the biradical starts to fragment. As the molecule relaxes along $\mathbf{MEP^S}$ and twists, the triplet $^3(2\pi)$ state becomes degenerate with S_0, and this degeneracy is maintained into the biradical region, where the minima on the $^1(2\pi)$ and $^3(2\pi)$ surfaces virtually coincide (compare structures **f** and **g**, **k** and **l**). However, single point calculations on the $^3(3\pi)$ energy surface computed along the $\mathbf{MEP^S}$ coordinate (see Figure 7 in the Supporting Information for details) indicate that it remains *parallel* to the $\mathbf{MEP^S}$ and some 3−5 kcal mol^{-1} higher in energy. Thus along this path the chemically relevant $^1(4\pi)$ and $^3(3\pi)$ energy surfaces *do not* cross. It appears that the double-well surface topology of the S_0 and $^3(3\pi)$ surfaces extends all the way from *syn* $\mathbf{MAX^S}$ to $\mathbf{BIR^S}$ (see Figure 2b,c), such that a crossing can occur anywhere along the $\mathbf{MEP^S}$ as soon as a step along the O−C−C asymmetric bending coordinate is taken. This implies the presence of an energetically accessible *crossing seam*, indicated in Figure 2a by a dashed line. The SOC computed between the S_0 ($^1(4\pi)$ or $^1(2\pi)$) and T_1 ($^3(3\pi)$) surfaces at each point along the $\mathbf{MEP^S}$ path was found to be large (60−70 cm^{-1}), indicating efficient intersystem crossing (ISC) would occur between these surfaces. However, ISC is not expected to be efficient between the S_0 ($^1(4\pi)$ or $^1(2\pi)$) and the $^3(2\pi)$ energy surfaces, as the SOC is virtually zero (<1 cm^{-1}) at all points along the $\mathbf{MEP^S}$.

Biradical Fragmentation Region. There appear to be virtually no barriers to fragmentation on the $^1(4\pi)$ surface. A

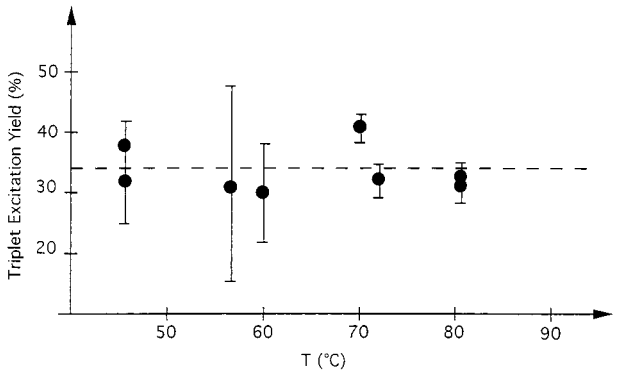

Figure 5. Triplet quantum yields (Φ^T) measured at different temperatures for the decomposition of TMD.

gauche transition state (structure **o**) leading from the gauche $^1(4\pi)$ minimum (structure **e**) to ground state products could not be fully optimized but indicates that the barrier to fragmentation is only about 0.5 kcal mol^{-1}. The corresponding *anti* transition structure could not be located at all, suggesting there is almost no barrier for fragmentation from the *anti* minimum.

The transition states (**TS$_2$**) for biradical fragmentation on the $^3(3\pi)$ energy surface were located at both *gauche* (structure **p**) and *anti* (structure **q**) geometries, the energy difference between the two transition state conformers being less than 2 kcal mol^{-1}. The energy required for dissociation from the *anti* triplet biradical is 4.7 kcal mol^{-1} including thermal correction. The computed minimum energy paths (**MEP^T**) from both *anti* and *gauche* conformers of **TS$_2$** lead to **BIR^T** in one direction, and n$-\pi^*$ triplet excited state formaldehyde in the other.

In conclusion we have shown the following: (a) The $^3(3\pi)$ and $^1(4\pi)$ energy surfaces *do not* cross along **MEP^S**. Instead, there is a line of $S_0/^3(3\pi)$ intersection leading from the O$-$O cleavage region to the biradical region, which can be accessed by O$-$C$-$C deformations, orthogonal to the reaction coordinate. (b) The SOC between the S_0 ($^1(4\pi)$ or $^1(2\pi)$) and $^3(3\pi)$ states is large, and therefore the $^3(3\pi)$ biradicals can be thermally populated via ISC by traversing the crossing in the O$-$O cleavage region. (c) The crossing seam terminates in the region of the $^3(3\pi)$ biradical, such that these biradicals can either go through **TS$_2$** and fragment, leading to excited state products, or decay (by facile ISC) to the S_0 biradical region and fragment, forming ground state products. (d) The $^1(4\pi)$ biradicals are *unstable* and can therefore fragment in an essentially barrierless process.

Mechanism of Triplet-Excited Product Formation and Comparison with the Experimental Data. Energy barriers for the triplet reaction were accurately measured by Adam *et al.*[3] for the parent and all possible methyl-substituted dioxetanes and were found to fall between 22 and 28 kcal mol^{-1}. Moreover, the triplet excitation yield ($\Phi^T = [P^T]/[D]$, where [D] is the amount of reacted dioxetane and [P^T] is the amount of triplet carbonyl product generated) is essentially temperature independent for TMD, as reported in Figure 5. This indicates a common rate-determining step for the triplet and ground state decomposition. This conclusion is in agreement with the measurements made by Steinmetzer and Turro.[7] They found that the activation energy for the disappearance of TMD is identical to the activation energy for the formation of both ground state and triplet acetone products. The same behavior has been observed in DED.[8] Furthermore, dissociation from the singlet $^1(3\pi)$ surface also appears to have the same activation energy in TMD,[7] although the singlet excitation yield Φ^S (and therefore also the chemiluminescence yield) is very small. These experiments all suggest that in dioxetanes the same activation barrier must control both the ground and excited state pathways of the reaction.

SCHEME 2

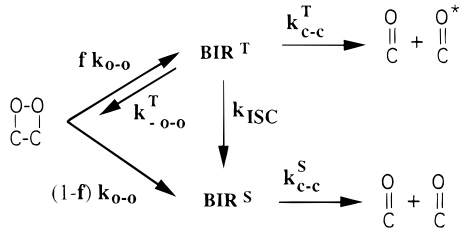

The structure of the S_0 and T_1 potential energy surfaces documented in the previous subsection allows one to derive a mechanistic model for singlet and triplet dioxetane decomposition, based upon conclusions (a)$-$(d). This model is given in Scheme 2. As pointed out in the Introduction, our computations yield an O$-$O cleavage activation barrier that is 6 kcal mol^{-1} lower than the experimentally observed value. Although this error seems unexpectedly large for the level of theory used in this work, it is generally recognized to be computationally difficult to evaluate the stability of strained rings with respect to open structures, and therefore we put this discrepancy down to methodological error.

Therefore we assume that O$-$O cleavage occurs exclusively on the ground state surface, in agreement with the generally accepted mechanistic view of Figure 1b. However, since no S_0/T_1 crossing is located along the computed S_0 reaction coordinate (see Figure 2a), one must explain the highly efficient chemienergization and production of triplet species. According to the results (a) and (b), ISC to the triplet surface can easily occur after the transition state, somewhere along **MEP^S** after passage through **TS$_1$**. In fact, since the computed **MEP^S** does not have components along the C$-$C fragmentation coordinate, fragmentation cannot be "direct"; i.e., there must be some redistribution of energy within the vibrational modes of the molecule first. Thus, given the large region of space spanned by the crossing line (see Figure 2b and related discussion) and the energetically facile distortion that the molecule must achieve to enter it, we believe that ISC from S_0 to the $^3(3\pi)$ surface can be efficient and compete with singlet fragmentation. This point is illustrated in Scheme 2, which shows that production of **BIR^T** and **BIR^S** occurs competitively and is controlled by the same rate constant k_{O-O} (i.e., dioxetane O$-$O cleavage). The actual branching ratio cannot be estimated from our analysis, and we indicate it by *f*.

After the triplet biradical **BIR^T** has been generated, fragmentation can be achieved as the O$-$O cleavage and the triplet fragmentation barriers have similar magnitudes (associated with a rate constant k^T_{C-C}). In fact, the efficiency of triplet fragmentation observed experimentally suggests that **TS$_2$** lies lower in energy than **TS$_1$**, which, as we discussed earlier, we believe is underestimated. According to Figure 2a, **BIR^T** exists in a deep energy well with a 5 kcal mol^{-1} barrier to either fragmentation or ring-closure (rate constant k^T_{O-O}). Such an intermediate may be trapped. However, the result (c) indicates that the bottom of the T_1 energy surface is leaking (due to efficient ISC to S_0), leading to decay to **BIR^S**. (d) indicates that the **BIR^S** biradical will fragment as soon as it is formed (i.e., the rate constant k^S_{C-C} is large). In conclusion, we expect a short lifetime for **BIR^T** as any triplet biradical that does not fragment immediately will efficiently branch to **BIR^S** via ISC (rate constant k_{ISC}). Thus our reaction mechanism is consistent

with the lack of observed chemical trapping of any biradical species.[9a] The TMD and TED tetraalkylated triplet biradicals are likely to have much smaller fragmentation barriers than the computed 4.7 kcal mol^{-1} barrier in the parent dioxetane **BIR^T**. This implies that, in these compounds, k^T_{C-C} may be substantially larger than k_{ISC}, leading to an even shorter lifetime for **BIR^T** and a substantial temperature independence of the triplet excitation yield consistent with the experimental data in Figure 5. Unfortunately, the temperature dependence of Φ^T has never been investigated for less substituted dioxetanes than TMD.

Finally, let us comment on the mechanism of the dioxetane decomposition reaction from a more chemical point of view. The *merged mechanism* was previously proposed[3] to unify the concerted and the two-step biradical pathways in order to rationalize the large amount of kinetic and product data. This mechanism implies that dioxetane decomposition involves passage through an extremely asynchronous transition state that incorporates features of both the biradical and concerted paths. For the parent dioxetane investigated here, we propose that at the merging point, a short-lived (<10 ps), metastable triplet biradical appears to intervene,[9a] which should be detectable by femtosecond spectroscopy.

Conclusions

The singlet and triplet state surfaces of dioxetane have been mapped out and the regions where they cross were examined. The energetics have been computed with various CASSCF active spaces with MP2 corrections in several basis sets. The computed energy barrier for the ring-opening of dioxetane is 16 kcal mol^{-1}, which is lower than the observed threshold (22 kcal mol^{-1}) for unsubstituted dioxetane decomposition. This is ascribed to methodological error, as it is generally recognized to be computationally difficult to reproduce ring-opening barriers in strained rings. More significantly, it is shown that the singlet and triplet surfaces do not actually cross along the S_0 reaction pathway (**MEP^S**) connecting the O−O cleavage transition state **TS$_1$** region to the biradical region, as expected. These results indicate that the mechanism of the dioxetane luminescent decomposition cannot be fully understood on the basis of a one-dimensional picture of the reaction coordinate (Figure 2a). On moving to a multidimensional picture of the potential surfaces involved, we find that a vast line of $S_0/^3(3\pi)$ crossing points spans the O−O cleavage valley. The SOC computed between the $S_0{}^l(4\pi)/^1(2\pi)$ and $^3(3\pi)$ surfaces is large (ca. 60−70 cm^{-1}); therefore the efficiency for ISC to the $^3(3\pi)$ energy surface should be high. Once on the $^3(3\pi)$ surface, fragmentation to form excited state products will compete with efficient ISC back to the ground state surface. The results suggest there is a four-level quasi-degeneracy between singlet and triplet (3π) and (2π) states, such that this ISC back to the $S_0{}^1(2\pi)$ surface will be extremely efficient. Therefore, the triplet biradical is expected to be too short-lived for chemical trapping.

While a valid mechanistic hypothesis for the parent dioxetane consistent with the present high-level computations is presented, it still needs to be substantiated by further theoretical and experimental studies on substituted 1,2-dioxetanes. Of interest would be femtosecond spectroscopy of the so far elusive **BIR^T** intermediate.

Acknowledgment. M.O. and M.A.R. are grateful to NATO for a travel grant (CRG 950748). This research has been supported in part by the EPSRC and SERC (U.K.) under grant numbers GR/J25123 and GR/H58070 and in part by an EU TMR network grant (ERB 4061 PL95 1290, Quantum Chemistry for the Excited State). S.W. is grateful to the EPSRC for a studentship. The Würzburg group thanks the Deutsche Forschungsgemeinschaft (SFB 172) and the Fonds der Chemischen Industrie for generous financial support. S.M. is grateful for an Alexander von Humbolt postdoctoral fellowship.

Supporting Information Available: Two pages including (i) Figure 6 reporting the energies of the $^1(4\pi)$ and $^3(3\pi)$ surfaces computed along the OC−CO torsional coordinate connecting *syn* **MAX^S** to **TS$_1$**, (ii) Figure 7 reporting the results of $^1(4\pi)/^1(2\pi)$, $^3(2\pi)$, and $^3(3\pi)$ computed energy profiles along the **MEP^S** coordinate connecting **TS$_1$** to the *gauche* biradical, **BIR^S**. This material is available free of charge via the Internet at http://pubs.acs.org.

References and Notes

(1) See: Adam, W. In *Chemical and Biological Generation of Excited States*; Adam, W., Cilento, G., Eds.; Academic Press: New York, 1982; pp 129−34 (see also references cited therein).

(2) Wilson, T.; Golan, E. E.; Harris, M. S.; Baumstark, A. J. *J. Am. Chem. Soc.* **1976**, *98*, 1086. Wilson, T.; Schaap, P. *J. Am. Chem. Soc.* **1971**, *93*, 4126.

(3) Adam, W.; Baader, W. J. *J. Am. Chem. Soc.* **1985**, *107*, 410.

(4) Reguero, M.; Bernardi, F.; Bottoni, A.; Olivucci, M.; Robb, M. A. *J. Am. Chem. Soc.* **1991**, *113*, 1566.

(5) Turro, N. J. *Modern Molecular Photochemistry*; Benjamin/Cummings Publishing Co.: Menlo Park, CA; 1978; p 597.

(6) Horn, K. A.; Koo, J.; Schmidt, S. P.; Schuster, G. B. Mol. Photochem. **1978−79**, *9*, 1−37.

(7) Steinmetzer, H.; Yekta, A.; Turro, N. J. *J. Am. Chem. Soc.* **1974**, *96*, 282.

(8) Wilson, T.; Schaap, P. *J. Am. Chem. Soc.* **1971**, *93*, 4126.

(9) (a) Richardson, W. H.; Lovett, M. B.; Olson, L. *J. Org. Chem.* **1989**, *54*, 3523. We have recently reexamined this claim and concluded against biradical trapping; cf.: Adam, W.; Murphy, S. *J. Am. Chem. Soc.* **1996**, *118*, 12916. (b) Smith, K. K.; Koo, J. K.; Schuster, G. B.; Kaufmann, K. J. *J. Phys. Chem.* **1978**, *82*, 2291.

(10) Our computations[4] have been recently questioned; cf.: Wilson, T.; Halpen, A. M. *J. Phys. Org. Chem.* **1995**, *8*, 359.

(11) Adam, W.; Andler, S. *J. Am. Chem. Soc.* **1994**, *116*, 5674.

(12) The MC-SCF program used is implemented in *Gaussian 94*, Revision B.2, by M. J. Frisch, G. W. Trucks, H. B. Schlegel, P. M. W.; Gill, B. G. Johnson, M. A. Robb, J. R. Cheeseman, T. Keith, G. A. Petersson, J. A. Montgomery, K. Raghavachari, M. A. Al-Laham, V. G. Zakrzewski, J. V. Ortiz, J. B. Foresman, C. Y. Peng, P. Y. Ayala, W. Chen, M. W. Wong, J. L. Andres, E. S. Replogle, R. Gomperts, R. L. Martin, D. J. Fox, J. S. Binkley, D. J. Defrees, J. Baker, J. P. Stewart, M. Head-Gordon, C. Gonzalez, and J. A. Pople (Gaussian, Inc.: Pittsburgh, PA, 1995).

(13) Peasley, K.; McDouall, J. J. W.; Robb, M. A. *Chem. Phys. Lett.* **1988**, *148*, 183.

(14) (a) Andersson, K.; Malmqvist, P.-A.; Roos, B. O. *J. Chem. Phys.* **1992**, *96*, 1218. (b) MOLCAS, Version 3, K. Andersson, M. R. A. Blomberg, M. Fülscher, V. Kellö, R. Lindh, P.-A. Malmqvist, J. Noga, J. Olsen, B. O. Roos, A. J. Sadlej, P. E. M. Siegbahn, M. Urban, P. O. Widmark (University of Lund: Lund, Sweden, 1994).

(15) (a) Ragazos, I. N.; Robb, M. A.; Bernardi, F.; Olivucci, M. *Chem. Phys. Lett.* **1992**, *197*, 217. (b) Yarkony, R. D. *J. Phys. Chem.* **1993**, *97*, 4407. (c) Bearpark, M. J.; Robb, M. A.; Schlegel, H. B. *Chem. Phys. Lett.* **1994**, *223*, 269.

(16) Koseki, S.; Schmidt, M. W.; Gordon, M. S. *J. Phys. Chem.* **1992**, *96*, 10768.

(17) Harding, L. B.; Goddard, W. A., III *J. Am. Chem. Soc.* **1997**, *99*, 4521.